THE ASTROPHYSICAL JOURNAL SUPPLEMENT SERIES, 73:333–342, 1990 June


# NEUTRAL BEAMS IN TWO-RIBBON FLARES AND IN THE GEOMAGNETIC TAIL

P. C. H. MARTENS AND A. YOUNG
Harvard-Smithsonian Center for Astrophysics
*Received 1989 February 6; accepted 1989 July 10*

## ABSTRACT

We study the current sheet created in the wake of an erupting filament during a two-ribbon flare. A comparison with the geomagnetic tail shows that the physics of these systems is very similar, and therefore the existence of super Dreicer fields and the generation of neutral beams traveling down the postflare loops with small pitch angles may be expected.

The observational evidence for neutral beams in flares is reviewed and found to be generally supportive, while contradicting the widely held hypothesis of electron beams. A dimensional analysis further demonstrates that the results for self-consistent numerical simulations of the current sheet in the geomagnetic tail can directly be scaled to the coronal current sheet, and the scaling parameters are derived.

*Subject headings:* hydromagnetics — particle acceleration — Sun: flares — Sun: particle emission

## I. INTRODUCTION

The eruption of filaments is often considered as the physical cause for two-ribbon flares (Carmichael 1964; Van Tend and Kuperus 1978). In the Kopp and Pneuman model (1976) and its successive refinements (Pneuman 1980; Anzer and Pneuman 1982) it is surmised from the observed formation of postflare loops that a current sheet forms in the wake of the erupting filament. It also is believed that in this current sheet free magnetic energy is converted into particle kinetic energy. The particle kinetic energy is either in the form of a superhot thermal plasma, or in the form of electron beams, or, perhaps, proton beams. Flare loops are formed in this current sheet through reconnection of field lines that originally overlie the erupting filament (see Martens and Kuin 1989 for a drawing of the field configuration and the location of the energy conversion processes). As these loops are formed, energized particles from the current sheet may be injected at the tops of the loops and generate the radiative flare products—from X-rays to radio—through various processes.

This scenario for two-ribbon flares has recently served as a useful framework for interpreting simultaneous observations of large flares in X-rays, radio, and H$\alpha$ (Dennis 1985; Cliver *et al.* 1986). In addition, numerical simulations with a full MHD–code (Mikic *et al.* 1988) have demonstrated the formation of a current sheet below an erupting helical flux tube, and a simplified circuit code for filament eruptions and current sheet formation (Martens and Kuin 1989) reproduced the magnetic field evolution in a two-ribbon flare in considerable detail.

Although a consensus seems to be emerging on the global scenario for two-ribbon flares, two key elements remain far from being understood: (1) what is the precise physical mechanism for the conversion of free magnetic energy to particle kinetic energy, and (2) how is the particle kinetic energy transported along the loops and converted into radiative flare products; in particular, how are the hard X-rays produced?

The literature on this subject has long been dominated by the debate on the "thermal" versus the "nonthermal" hypothesis (see Vilmer 1987 or Dennis 1988 for a recent review). In the former it is assumed that somehow a very hot ($10^8$ K) plasma is generated in the sheet and injected into the loops. The observed hard X-rays are then directly radiated from this superhot plasma as it rapidly cools down. In the latter hypothesis electron beams are generated presumably by direct electric field acceleration (for example in current sheets or in double layers). These beams then generate "thick-target" hard X-rays upon impact on the chromosphere, after traveling downward along the loops, or they generate "thin target" emission when interacting with the coronal plasma inside the loops.

The observations of the hard X-ray imaging spectrometer (HXIS) aboard *SMM* seem to support the electron beam hypothesis (see Hoyng *et al.* 1981 and Duijveman, Hoyng, and Machado 1982), but alternative interpretations remain viable (see MacKinnon, Brown, and Hayward 1985). On the theoretical side there are many problems with both hypotheses. On one hand, it is not at all clear how a superhot thermal plasma can be formed in coronal current sheets. On the other hand, the propagation of electron beams along coronal loops poses many problems with regard to their stability, and the necessity of cospatial return currents (see Vilmer 1987 for a recent review).

In the present paper we will explore the third alternative: neutral beams, with equal amounts of protons and electrons traveling at the same speed. We do not propose a complete theory here, from the formation of the beams to the emission of hard X-rays, but we do present a fairly complete picture of the formation of the neutral beams, and we also interpret several observations that seem to indicate the existence of neutral beams in flares. Neutral beams were originally proposed by Simnett and Strong (1984) and Simnett (1986), because they would explain several observations, such as the

timing of the chromospheric upflows versus the hard X-rays, much better than either electron beams or a superhot plasma. Recently Martens (1988*a*, *b*) and Martens and Young (1989) demonstrated an acceleration mechanism for these beams that is analogous to the acceleration mechanism that operates in the geomagnetic tail (Speiser 1965, 1967, 1968; see Lyons and Williams 1984 for a recent review). Here we will continue our analysis from these results.

This paper is organized as follows. In § II we present a brief summary of the acceleration mechanism and analyze the theoretical and observational evidence for the existence of strong electric fields in flares, which are crucial for this acceleration mechanism. A three-way comparison is made between the physical parameters of the coronal current sheet, the geomagnetic tail, and a laboratory current sheet (Stenzel *et al.* 1985).

In § III we discuss three independent tests for neutral beams with protons in the 100 KeV range: (1) the observation of redshifted Ly$\alpha$ radiation, (2) the measurement of the polarization of line emission caused by the beam impact ionization in H$\alpha$ and (3) in the SI$\lambda$1437 line. We also summarize the evidence for neutral beams offered by Simnett (1986), and the measurement of an upper cutoff in proton spectra (Heristchi, Trottet, and Perez-Peraza 1976), consistent with the present model.

Finally, in § IV, we consider the requirements for fully self-consistent models of the current sheet. We emphasize that the familiar MHD–description is inadequate here, since the effects finite proton gyroradius are not negligible in the sheet (as is assumed in MHD). Instead we model the collisionless current sheet by following individual particles in their orbits and by calculating the currents and magnetic fields generated by these motions. Such simulations have been carried out for the geomagnetic tail (see the review by Hockney and Eastwood 1988, chap. 9-4), but not for the sheet in two-ribbon flares.

In the final section of this paper the main conclusions are summarized and future observations are suggested.

## II. THE PARTICLE ACCELERATION MECHANISM

To explain the observed hard X-ray emission from flares as the result of the impact of a particle beam on the dense chromosphere, the mean energy of the particles has to be $\sim 30$ KeV if the beam is composed of electrons (Lin and Schwartz 1987), and 200 KeV if protons are the carriers of the beam energy (Simnett 1986). After acceleration in the current sheet, the mean free path for momentum loss by the electrons as well as the protons would be $\sim 10^{10}$ cm, equal to the length of the whole erupting structure. [We have corrected here for the omission of a factor $(m_e/m_p)^{1/2}$ in eq. (2) of Martens (1988*a*) for the mean free path of protons. Explicit expressions for the calculation of the m.f.p.'s are given in Trubnikov (1965). Other quantities discussed below are correctly calculated in Martens (1988*a*), and these calculations shall not be repeated here.]

Given the particle energies, and an estimate of the electric field strength in the sheet of 2 V cm$^{-1}$, inferred from the observed photospheric field strength and ribbon velocities (Kopp and Poletto 1986), one can easily calculate the acceleration length of the particles in the sheet, by equating the required particle energy to the potential drop in the sheet over an acceleration length (Martens 1988*b*). The result for the solar sheet is an acceleration length of the order of $10^5$ cm, five orders of magnitude smaller than the mean free path. The actual mean free path of the particles may be two or at most three orders of magnitude smaller than $10^{10}$ cm, because of collective (e.g., wave-particle) interactions, giving rise to anomalous resistivity, but an increase of five orders is unlikely for anomalous processes.

It appears therefore that the particles do not interact during their acceleration process, and one has to consider a different way to limit the acceleration path to $\sim 10^5$ cm. This situation is quite similar to that in the geomagnetic tail, where also the electric field is much larger than the Dreicer field and the mean free paths for protons and electrons are many orders of magnitude larger than the tail's dimensions (see Lyons and Williams 1984 for a review). Early model calculations (Speiser 1965, 1967) prompted in *in situ* satellite measurements of electric and magnetic fields have shown that in the geomagnetic tail the "guiding center" approach for proton orbits—in which the gyration of the protons is "averaged out"—is not valid in the sheet because the magnetic field changes significantly over one proton gyroradius. A similar situation may be expected in the current sheet created in the wake of an erupting filament (Martens 1988*a*, *b*).

In this situation the orbits of individual protons must be calculated by explicit integration of their equation of motion

$$m_p \frac{dV}{dt} = e\left(\boldsymbol{E} + \frac{\boldsymbol{V}\times\boldsymbol{B}}{c}\right). \tag{1}$$

Here it is supposed that $\boldsymbol{E}$ is constant and directed along the axis of the sheet, while $\boldsymbol{B}$ consists of two components: one tangential to the sheet, that changes sign across the sheet ($B_s$), and a small component ($B_p$) perpendicular to the sheet (see Fig. 1). The numerical and approximately analytical solutions by Speiser (1965) demonstrate the following behavior for the proton and electron orbits:

1. Before entering the sheet the particle orbits can be integrated analytically. The results show the familiar gyromotion, $\boldsymbol{E}\times\boldsymbol{B}$ drift, and constant velocity motion along the field lines (Sivukhin 1965).

2. After entering the sheet the motion consists of three components: first there is a rapid oscillation around the midplane of the sheet, where the tangential field component and hence the sense of gyration changes sign. Second, the particles are accelerated along the electric field. If there were not a perpendicular field component in the sheet this acceleration would be uninhibited, and the particle would traverse the length of the whole sheet (Speiser 1965). However, in the presence of a $B_p$, the particle is deflected by the perpendicular field component as it acquires a velocity component parallel to the electric field. The result is a gyration with a very large radius

$$r_p = \frac{m_p \bar{V} c}{eB_p}, \tag{2}$$

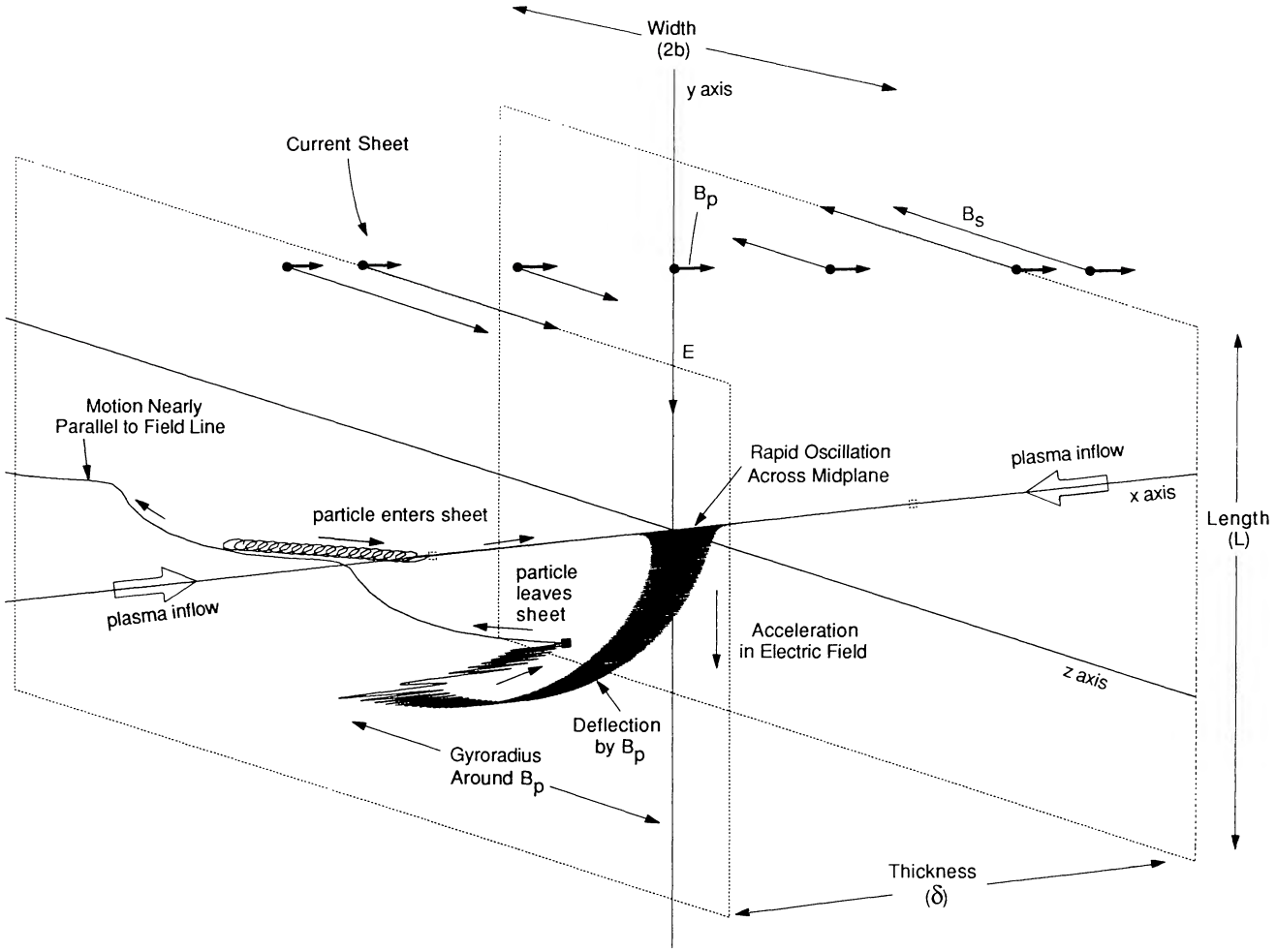


FIG. 1.—A Typical proton orbit in the current sheet of a two-ribbon flare. Inside the sheet the motion along the $\hat{y}$ and $\hat{z}$ axes is scaled down by a factor 250, respectively, 500 for clarity of presentation.

in the midplane of the sheet, in addition to the much more rapid oscillation perpendicular to the sheet. Here $\bar{V}$ denotes the average proton velocity in the sheet. Speiser's (1965) results demonstrate that after a 90° deflection in the midplane the particle is again ejected from the sheet (see also Fig. 1).

3. After ejection from the sheet the particle orbit is fully integrable again. The velocity of the ejected particles is nearly parallel to the magnetic field with magnitude (Speiser 1965)

$$V_{\text{beam}} = \frac{2Ec}{B_p}. \tag{3}$$

The average proton velocity in the sheet, $\bar{V}$ in equation (2), is about equal to about half the beam velocity $V_{\text{beam}}$, so an expression for $r_p$ in terms of sheet parameters may be derived

$$r_p = \frac{m_p Ec^2}{eB_p^2}. \tag{4}$$

The above characteristics are clearly exhibited in Figure 1, which shows the results of the numerical integration of a proton orbit with parameters typical for the solar corona (Table 1). One recognizes the rapid oscillation across the midplane, as well as the acceleration parallel to $\boldsymbol{E}$, and the deflection because of $B_p$. It is important to note here the following characteristics of this acceleration mechanism:

1. Protons and electrons acquire the *same* final velocity, and both leave the sheet almost parallel to the magnetic field. Hence high-velocity neutral beams leave the sheet from *the same sides* as where the plasma is initially convected into the sheet, in contrast to the situation in a standard collisionally dominated current sheet, where the plasma is "squeezed" out from the top and the bottom of the sheet. As was demonstrated above, the particles in the neutral beams are collisionless, which explains why these beams can propagate through the incoming plasma. *Inside* the sheet protons and electrons are of course accelerated in opposite directions, but the outgoing beams are neutral since the electrons and protons are both ejected from the sheet parallel to the field lines, and with the same velocity (see Figs. 2 and 3 of Speiser 1965). Because protons are much heavier than electrons, protons carry the bulk of the beam energy.

TABLE 1

COMPARISON BETWEEN PLASMAPHYSICS OF GEOMAGNETIC TAIL, CURRENT SHEET IN A TWO-RIBBON FLARE, AND STENZEL'S CURRENT SHEET EXPERIMENT.

| Physical Quantity | Geomagnetic Tail | Two-Ribbon Flare | Laboratory |
|---|---|---|---|
| | | Observations | |
| Sheet magnetic field | $2\times10^{-4}$ G (1,2) | 200 G (3) (typical for active region) | 12 G (14) |
| Sheet electrical field | $2.5\times10^{-6}$ V cm$^{-1}$ (1) | 2 V cm$^{-1}$ (4,5) | 0.1 V cm$^{-1}$ (14,15) |
| Energy of accelerated protons | 2–100 KeV (1,6) (power law) | 200 KeV–MeV range (7) (inferred from hard X-Rays) | N.A. |
| Sheet length | $2.6\times10^{10}$ cm (8) | $1.2\times10^{10}$ cm (9) (inferred from filament length) | 180 cm (14) |
| Sheet width ($\neq$ thickness!) | $1.3–13\times10^{10}$ cm (8) | $10^{9}$ cm (9,10) (inferred from width ribbons) | $\approx$ 40 cm (14,15) |
| Density of ambient plasma | 0.02–5 cm$^{-3}$ (11) | $10^{10}$ cm$^{-3}$ (12) (typical for active region) | $10^{12}$ cm$^{-3}$ (14) |
| Temperature of ambient plasma | $1.5\times10^{6}$ K (13) | $2.0–3.0\times10^{6}$ K (12) (typical for active region) | $T_e \approx 1.2\times10^{6}$ K ($T_p \approx 0.2\ T_e$) (14) |
| | | Dimensionless Quantities | |
| Number of particles in Debye sphere | $4.0\times10^{12}$ | $3.9\times10^{7}$ | $3.4\times10^{4}$ |
| Plasma $\beta$ (outside sheet) | $5.2\times10^{-3}$ | $4.3\times10^{-3}$ | 2 |
| Plasma Frequency/Gyrofrequency | 9 | 1.6 | 267 |
| Sheet thickness/proton gyroradius before acceleration | 34 (1) | 52 | 0.83 (14) |
| Electric field/Dreicer field | $1.2\times10^{8}$ | $6.7\times10^{3}$ | 0.15 |
| Parallel/perpendicular component magnetic field | 20 (1) | 290 | not measured |
| Effective resistivity/ Spitzer resistivity | $1.4\times10^{9}$ | $3.0\times10^{6}$ | 25 |
| Observed/calculated proton energy after acceleration | 1.5 | 1.2 | N.A. |

REFERENCES.—(1) Lyons and Williams 1984; (2) Ness 1965, (3) Poletto *et al.* 1975; (4) Kopp and Poletto 1986; (5) Foukal, Little, and Gilliam 1987; (6) Lundin *et al.* 1981; (7) Simnett 1986; (8) Speiser and Ness 1967; (9) Kaastra 1985; (10) Martens and Kuin 1989; (11) Akasofu *et al.* 1973; (12) Rosner, Tucker, and Vaiana, 1978; (13) Rosenbauer *et al.* 1975; (14) Stenzel, Gekelman, and Urrutia 1985; (15) Stenzel, Gekelman, and Wild 1983.

2. This acceleration mechanism is essentially a finite gyroradius effect, which cannot be found from classical MHD. Free magnetic energy is converted to particle kinetic energy in the form of neutral beams without collisions or wave-particle interactions. Speiser (1987) refers to this process as "inertial dissipation." The resulting dissipation coefficients are orders of magnitude larger than the classical Spitzer collisional resistivity; an explicit calculation is given below.

The results of the numerical calculations of Speiser (1965) have been applied to the solar case. The results of this analysis (Martens 1988*a*) are

1. The drift of plasma into the sheet continuously supplies the needed $4\times10^{35}$ protons s$^{-1}$.

2. The sheet magnetic field ($\sim$ 200 G) generated by the proton current is acceptable despite the large number of accelerated protons and electrons. This stands in contrast with the result of Hoyng, Brown, and Van Beek (1976) for electron beams in single loops. The reason for this difference is that the current sheet in Martens's calculations is situated at the top of an *arcade* of coronal loops, as in the Kopp and Pneuman (1976) model. At any cross section of this sheet only a tiny fraction of the total number of accelerated protons and electrons passes through: the fraction that entered the sheet within one acceleration length ($\approx10^{5}$ cm) before the cross section. The other particles have already been ejected from the sheet before reaching the cross section, or enter behind it. The result of Hoyng *et al.* (1976) is still valid in a single loop geometry.

3. The result that neutral particle beams are injected at the top of the arcade of loops, with almost zero pitch angle, greatly reduces the problems for their propagation: there is no need for return currents, so there are far fewer potential beam instabilities, and mirroring is not significant.

4. The generation, timing, and spatial distribution of $\gamma$-rays and hard X-rays, may be explained from a single power-law proton spectrum, generated by this acceleration mechanism, with cutoffs at $\sim$ 200 KeV and 20 GeV. These cutoffs will be discussed in more detail in § III.

5. The enormous *effective* resistivity in the current sheet, over five orders of magnitude larger than the classical collisional Spitzer resistivity, eliminates the discrepancy between the theoretical values for coronal resistivity, and the values indirectly inferred from observations.

Crucial in the derivation of the above results is the large electric field strength of 2 V cm$^{-1}$, five orders of magnitude larger than the Dreicer field in the solar corona. Kopp and Poletto derived this estimate from the $\boldsymbol{V}\times\boldsymbol{B}$ field determined by the lateral displacement of the flare ribbons across the normal component of the photospheric magnetic field. Their measurements apply to the preflare, impulsive, and postflare

phase of the large 1973 July 29 two-ribbon flare. The electric field peaks at the onset of the impulsive flare. It was shown by Forbes and Priest (1984) that in a system with an ignorable coordinate along the filament axis (as is indicated by observations), the electric field at the X-type neutral line is exactly the same as near the ribbons for stationary reconnection. Note that this electric field is *perpendicular* to the magnetic field, except at the neutral point, where there is no magnetic field. It was also shown by Kopp and Poletto (1986) that in the absence of perfect symmetry along the neutral line, the net potential drop along the current sheet is still equal to the flux increase in the postflare loop system through the lateral motion of the flare ribbons.

This result is in contrast with the results of experiments in laboratory plasmas, where the electric field is usually limited to the Dreicer field (e.g., Stenzel, Gekelman, and Wild 1983; Stenzel, Gekelman, and Urrutia 1985). On the other hand, the electric field in the geomagnetic tail, determined by *in situ* observations of the reconnection rate, is about eight orders of magnitude larger than the Dreicer field. In the experiment of Stenzel the net electric field in the neutral sheet consists of two parts, an inductive part generated by the magnetic reconnection, and a space charge part, generated by charge build up at the anode and cathode at the endpoints of the sheet. The space charge electric field counteracts the inductive field in such a way that the net field is limited to the Dreicer field.

The current sheets in a two-ribbon flare and the geomagnetic tail are not bounded in the way a laboratory plasma is, and therefore charge separation at the endpoints of the sheet is not possible. For example, charge separation at the endpoints of the flare current sheet would immediately be canceled by removal of the excess charge carriers along the field lines of the postflare loops connecting to the—for all practical purposes—infinite reservoir of particles in the chromosphere and photosphere. Consequently the net electric field is completely determined by the reconnection rate of the magnetic field.

Therefore it appears that large electric fields in the current sheet below an erupting filament can only be avoided when there is no reconnection at the top of the postflare loops. This would imply that the same arcade of loops remains connected to the X-type neutral line during the flare, and its footpoints would not change position, in contrast to the observed lateral motion of the ribbons. However, it is possible that the observed H$\alpha$ ribbons have nothing to do with loops that are connected to the current sheet. Instead, some MHD instability can be envisaged to take place at sequentially higher and higher loops that already existed before the flare. The ribbons then still are the chromospheric signature of the energy release within each subsequent arcade of loops. In this picture the whole preflare structure would simply be stretched out during the flare, without any change in topology.

There are several possible observations that could determine whether the reconnection or the stretching picture is correct. The first one is by directly measuring the electric field during flares: a field of several V cm$^{-1}$ would imply reconnection. A second straightforward test is the observation of changes in topology. Suppose one can observe a preflare loop overlying the filament before eruption, and determine its footpoint positions. If, during or after the eruption, the ribbons at the footpoints of the postflare loops cover or go beyond the footpoints of the preflare loop, reconnection *must* have taken place.

We are not aware of any direct observation of topology changes, but electric field measurements have recently been attempted. Using observations of Stark broadening in Balmer and Paschen lines Foukal, Miller, and Gilliam (1983), Foukal, Hoyt, and Gilliam (1986), and Foukal, Little, and Gilliam (1987) have derived an upper limit of $\sim 10$ V cm$^{-1}$ for the macroscopic electric field in eruptive prominences and postflare loops. Future observations of the polarization of Paschen lines may result in an upper limit of substantially less than 10 V cm$^{-1}$, and thus the results of Kopp and Poletto may be verified.

We conclude that the presence of super Dreicer fields in two-ribbon flares is not unambiguously demonstrated from observations but does provide the most straightforward interpretation of the observations of the formation of postflare loops, and is also suggested by the presence of super Dreicer fields in the similar circumstances of the geomagnetic tail.

A three-way comparison between the physical situation in the current sheet of a two-ribbon flare, the geomagnetic tail and the laboratory plasma experiment of Stenzel *et al.* (1983, 1985) is presented in Table 1. The first part of the table gives the observed quantities and their references. From these, and assuming that the beam generation mechanism of Speiser (1965, 1967) is at work, one can calculate the sheet physical parameters such as the drift velocity, the mean free paths, the proton acceleration length, the effective resistivity, number of accelerated protons, net current, etc. (see Martens and Young 1989 for the results for the geotail and the corona). With these results the dimensionless parameters of the second part of Table 1 can be calculated.

The effective resistivity given in Table 1 is derived from the following consideration. The proton acceleration inside the sheet is limited by whatever mechanism ejects the protons from the sheet. Using the definition of the proton current density, $j = n_p e V_p$ one finds for the *effective* resistivity, defined as the ratio between the electric field and the current density (see Martens 1988*b*),

$$\eta_{\rm eff} = \frac{m_p V}{n_p e^2 (mfp)} . \tag{5}$$

The mean free path for proton-proton collisions is very large, so collisions are a very ineffective limiter. As was shown above (see Fig. 1), the acceleration path of the protons is limited to $\sim 1$ deflection radius in the midplane of the sheet, (eq. [4]), much less than the collisional mean free path. Replacing the mean free path by this radius and $V$ by $V_{\rm beam}/2$, equation (3), one finds for the *effective* resistivity

$$\eta_{\rm eff} = \frac{B_p}{n_p e c} . \tag{6}$$

A more detailed derivation of $\eta_{\rm eff}$, and in particular its dependence upon the initial values of $V_p$ is given in Lyons

and Speiser (1985). A peculiar aspect of their results is that protons with very high initial velocities are actually decelerated in the sheet, and hence their $\eta_{\rm eff}$ is negative. For the laboratory experiment $\eta_{\rm eff}$ is found as the ratio between current density and electric field.

The crucial parameter in this expression for the effective resistivity, as well as in the expression for the beam velocity (eq. [3]), is the strength of the perpendicular magnetic field component, $B_p$. The value of $B_p$ in the geomagnetic tail has been measured directly and is in good agreement with the observed proton velocities. In the solar corona such a measurement is impossible at the moment. However, a theoretical expression for $B_p$ in terms of more readily estimated parameters can be derived from Eastwood's (1972) consistency condition (see also Speiser 1984). This consistency condition stems from the demand that the electrical current found from the summation over individual particle orbits has to be the same current as is implied in the originally assumed sheet magnetic field. (We will explore this condition in detail in § IV). Eastwood derives that the beam velocity has to be equal to the Alfvén velocity at the edge of the sheet,

$$\frac{B_s}{\sqrt{4\pi m_H n_p}} = \frac{2Ec}{B_p}. \tag{7}$$

From the estimates for $B_s$, $E$, and $n_p$ in the solar corona, given in Table 1, one derives $B_p \approx 0.7$ G. Using this result in equation (3) for the beam velocity, a typical proton energy of 200 KeV is found, as is required by observations (Simnett 1986), and which is consistent with the starting point of our analysis. For the geomagnetic tail the above expression is verified with the observed $B_p$.

The estimate for the thickness of the current sheet ($\delta$) in Table 1 is derived from the induction law with the assumption of a quasi stationary sheet (Martens and Young 1989)

$$\delta = \frac{\eta c^2}{2\pi V_d} \approx 430 \text{ cm}, \tag{8}$$

where $V_d$ is the plasma drift velocity into the sheet ($\approx$15 km s$^{-1}$). The sheet thickness for the geotail and coronal current sheet are calculated with equation (8) above. For the geotail the result is in agreement with spacecraft measurements, while in the corona direct experimental verification is impossible at this time. The thickness of the laboratory sheet is directly observed. The value for the proton gyroradius before acceleration is derived from the strength of the magnetic field at the edge of the sheet, and the thermal proton velocity in the ambient plasma.

The comparison of the dimensionless parameters for the three plasmas in Table 1 demonstrates that the geotail and the flare current sheet are quite similar, despite their greatly different dimensional parameters. Equally obvious is the great difference with Stenzel's plasma experiment, despite the greater similarity in dimensional parameters between the coronal current sheet and the experiment. In Stenzel's laboratory current sheet most of the current is not carried by protons, but by electrons. The net electric field is smaller than the Dreicer field because of the charge buildup at the anode and cathode, that cancels the inductive electric field. Our conclusion is that the particle acceleration process in the geomagnetic tail and in the current sheet of a two-ribbon flare, both astrophysical plasmas without walls and with nearly identical dimensionless characteristics, are likely to be similar.

## III. OBSERVATIONAL SIGNATURES OF NEUTRAL BEAMS

Protons have been proposed as the primary means of energy transfer in flares from early on (Carmichael 1964; Elliot 1964; Schatzman 1967), but in the last decade or two electron beams have been the main focus of attention. Recently Simnett and Strong (1984) and Simnett (1986) have argued that the electron beam hypothesis should be reexamined, because it fails to explain some key observations and because neutral beams provide a straightforward explanation for the same observations. Their main arguments are as follows.

1. *SMM* observations with the X-Ray Polychromator (XRP) of the Ca XIX ion (Antonucci *et al.* 1982; Antonucci, Gabriel, and Dennis 1984) show sometimes large nonthermal line broadening and high upflow velocities *prior* to the onset of the hard X-ray emission in flares. This requires large energy deposition in the chromosphere prior to the impulsive phase, and electron beams cannot do this without generating substantial thick-target X-ray emission, which is not observed. Proton beams *can* generate such heating without producing X-rays. A very hot thermal plasma that emits hard X-rays is produced only after the heating rate in the chromosphere due to the bombardment by protons surpasses a certain threshold (Fisher, Canfield, and McClymont 1985; Fisher 1987); this is the impulsive phase of the flare. (Note that in this scenario the X-ray emission is generated by thermal electrons).

2. X-rays generated by thick-target impact of electron beams should be anisotropic and polarized, in contrast to thermal X-rays. Observations show isotropy (Kane *et al.* 1980) from simultaneous stereoscopic data, and only small upper limits to polarization (Tramiel, Chanan, and Novick 1984) incompatible with electron beams. The data are fully compatible with the generation of a superhot plasma in the chromosphere by proton beams.

3. Observations with the *SMM* Gamma Ray Spectrometer (GRS) (Chupp *et al.* 1982; Forrest *et al.* 1981) demonstrate conclusively that high-energy protons ($\geq$ 30 MeV) must be present from the onset of the impulsive phase of $\gamma$-ray flares: the $\gamma$-rays are observed simultaneously with the hard X-rays within the time resolution of the GRS instrument (2 s.). The number of high-energy protons is at least two orders of magnitude larger than that of high-energy electrons (Ramathy and Murphy 1984). A single acceleration mechanism for both MeV and KeV protons (as proposed in this paper) seems more straightforward than two different, but exactly simultaneous, mechanisms for KeV-electrons and MeV-protons.

Valid proof for the existence of proton beams, however, can never be obtained from arguments against electron beams or plausibility arguments alone. Dennis (1988) has compared proton beams to the Loch Ness monster because all the evidence for their existence is of the above nature. The observational difficulty with hekta KeV protons is that they

do not generate X-rays upon impact, or $\mu$-waves during their transport, as deka KeV electrons do.

We take issue with Dennis's statement here by reviewing three independent observational tests for proton beams, two giving evidence for proton beams, and the other inconclusive.

Orral and Zirker (1976) and Canfield and Chang (1985) have investigated the interaction of proton beams with the partly ionized chromosphere. They find that the main source of L$\alpha$ wing emission is charge exchange from the proton beam followed by spontaneous bound-bound transitions of the beam atoms. The increase in L$\alpha$ wing emission that is predicted for typical beam fluxes and proton energies is several orders of magnitude larger than what has been observed from *Skylab* for two flares (Canfield and VanHoosier 1980), but "it is not at all clear that those observations were obtained at a time when we expect protons to be present during these events" (Canfield 1988). Hence no clear indication or counter indication for proton beams is found here. Future space-based measurements with UV spectrometers with a spectral resolution of 1% or better can resolve this question. We surmise that other radiation signatures from charge transfer with heavier ions are quite likely to exist.

Hénoux and Chambe (1990) calculated the polarization in the line emission of hydrogen atoms excited by a beam of protons or electrons. They found that the direction of vibration of the electric field vector generating the H$\alpha$ emission is polarized *parallel* to the incident beam for deka eV electrons and deka KeV protons. (The polarization depends mainly on the *velocity* of the beam particles, hence the $m_p/m_e$ energy ratio). Assuming beam incidence perpendicular to the solar surface, an Earth-bound polarimeter would observe maximum intensity in the flare site–center of disk direction (which is the projection of the radial direction). For deka KeV electrons and deka MeV protons the electric field vector is polarized in the plane *perpendicular* to the beam, and hence an earth-bound observer sees polarization perpendicular to the flare site–disk center direction.

Three chromospheric flares were observed at Meudon on 1982 July 11 (see the figures in Hénoux 1990), and the results clearly show polarization in the disk center direction for several H$\alpha$ emitting spots. The timing coincides with the period from the onset to the peak of the soft X-ray emission as observed by *GOES* 2, which corresponds to the impulsive phase. Hénoux *et al.* (1990) rule out deka eV electrons for two reasons: (1) the mean free path of these electrons is so small that they have to come from the transition region, which is unlikely, and, more important, (2) these electrons do not carry enough energy to power the simultaneous X-rays. Deka KeV electrons, and hence standard electron beams, are ruled out because they would cause polarization in the perpendicular direction to the one observed.

For typical preflare coronal values of $T \approx 2\times10^6$K, $n_e \approx 2\times10^9$ cm$^{-3}$, and the height of the current sheet at the onset of the flare of $\sim10^9$ cm (Martens and Kuin 1989; Takakura *et al.* 1986), one finds a preflare coronal column density of $\sim 4\times10^{-6}$ g cm$^{-2}$, less than model $F_1$ in Hénoux *et al.* (1990). From extrapolation of their results we find that the energy flux in the neutral beam that is required is to produce the polarization is $\sim10^{10}$ ergs cm$^{-2}$ s$^{-1}$, and the protons need to have an initial energy in excess of 200 KeV to reach the H$\alpha$-producing layer. This is in good agreement with the theoretical results of the previous section: there is a lower energy cutoff in the energy spectrum at 200 KeV, and with the power calculated in Martens and Young (1989) and a surface area of the ribbons of $\sim10^{19}$ cm$^2$ (length $10^{10}$ cm, width $5\times10^8$ cm), the predicted energy flux in the beams is $10^{10}$ ergs cm$^{-2}$ s$^{-1}$.

Similar observations of impact polarization in the SiI$\lambda$1437 line have been made with the *SMM* UVSP instrument (Hénoux *et al.* 1983). They found polarization up to 25% within 3° of the flare site–center disk direction, again implying impact by electrons in the deka eV range or protons in the deka KeV range, and again totally inconsistent with the polarization direction expected from deka KeV electron beams. A polarization of 9% was observed during the peak of the impulsive phase (the onset of the soft X-rays), and 25% polarization occurred during the decay phase of the flare, with no polarization in between. While the latter peak in polarization is most easily accounted for by impact of deka eV electrons carrying down heat flux from the hot and dense postflare loops as was proposed by Hénoux *et al.* (1983), the polarization at the onset of the flare cannot be explained this way, in the absence of preflare dense loops. Neutral beams, on the other hand, penetrate easily through the tenuous preflare plasma, as was demonstrated above. We thus submit that the flare-onset polarization is caused by neutral beams. This effect vanishes as the flare loops become denser through chromospheric evaporation, because the proton mean free path in the corona declines. Later on, in the postflare phase, heat flux–carrying electrons revive the polarization. Clearly, more observations are required to test this scenario.

Finally we will briefly discuss an older observation that supports the specific proton acceleration mechanism described in the previous section. The maximum attainable proton energy is defined by the full potential drop along the current sheet. With the electric field strength of 2 V cm$^{-1}$ and sheet length of $\sim10^{10}$ cm this maximum energy is $\sim$ 20 GeV. This should be regarded as an absolute upper limit, since only the largest two-ribbon flares have such long filaments. Observations of high-energy solar flare protons with the worldwide neutron monitor network in the early 1970s (Heristchi and Trotter 1971; Heristchi *et al.* 1976), have produced direct evidence for a high-energy cutoff in the proton spectrum in the range from 2 to 5 GeV for seven flares for which the cutoff energy could be calculated, close to our theoretical value.

## IV. SELF-CONSISTENT SHEET MODELS

In a self-consistent model one has to take into account that the currents are the result of the relative motion of the protons and the electrons; in other words, the net currents that are found by considering the summation over the individual particle orbits, need to be consistent with the currents in the originally assumed magnetic field. (In the calculations for Figure 1, $j_y = (B_s c/4\pi\delta)$ inside the sheet, and the current density vanishes outside the sheet.)

It may be shown that in a current sheet of the type of the geomagnetic tail the current is mainly carried by the protons,

because of their larger gyroradius, and that the electrons will move in such a way as to preserve charge neutrality, and prevent currents other than parallel to the sheet (Eastwood 1972, 1974). In this case the basic equations governing the formation and evolution of a sheet are

Faraday's law:

$$\frac{1}{c}\frac{\partial \boldsymbol{B}}{\partial t} = -\nabla\times\boldsymbol{E}. \tag{9}$$

Ampére's law:

$$\nabla\times\boldsymbol{B} = \frac{4\pi}{c}\boldsymbol{j}. \tag{10}$$

The momentum equation for the protons:

$$m_p\frac{d\boldsymbol{V}}{dt} = e\left(\boldsymbol{E} + \frac{\boldsymbol{V}\times\boldsymbol{B}}{c}\right). \tag{11}$$

The definition of the current density

$$\boldsymbol{j}\times\boldsymbol{E} = n_p e\bar{\boldsymbol{V}}\times\boldsymbol{E},$$

$$\boldsymbol{j}\times\boldsymbol{E} = \boldsymbol{0}, \tag{12}$$

where the bar indicates the local average over the velocity of all protons at that location and $n_p$ is the proton density, found from summation over the individual protons. Note that since this density is found from summation, mass continuity is automatically satisfied, and there is no risk of the density becoming negative at some point in space, as may happen in numerical simulations for the Eulerian formulation of the Vlasov or MHD equations (see Hockney and Eastwood 1988, chap. 9-4 for a detailed discussion of this approach). We note that in the actual simulations a single particle often represents many ($10^4$–$10^6$) actual protons, because of limitation in computer capacity.

We consider a sheet of the type drawn in Figure 1. The coordinates are $\hat{x}$ perpendicular to the sheet, and parallel to $B_p$; $\hat{z}$-parallel, respectively, antiparallel to the sheet magnetic field, and $\hat{y}$-parallel to the axis of the sheet, and parallel to the electric field. We assume $B_y = 0$ and $\partial_y = 0$. We explicitly allow for time variability and for variations in the $\hat{z}$-direction. Because of the absence of $y$-dependence, the magnetic vector potential can be reduced to one component,

$$\boldsymbol{B} = \nabla\times(A_y\hat{y}). \tag{13}$$

From Faraday's law, equation (10), and $\partial_y = 0$ it is found that $\boldsymbol{E}$ in the $x, z$-plane is a gradient type vector. However, because of the absence of charge separation ($\nabla\cdot\boldsymbol{E} = 0$) and vanishing $\boldsymbol{E}$ at large distances, it can be shown that $E_x = E_z = 0$, and hence Eastwood's (1972, 1974) result that $j_x = j_z = 0$ is rather plausible. Thus we have,

$$\boldsymbol{j} = (0, j_y, 0), \qquad \boldsymbol{E} = (0, E_y, 0), \qquad \boldsymbol{A} = (0, A_y, 0). \tag{14}$$

Ampère's law now reduces to

$$\nabla^2 A_y = -\frac{4\pi}{c}j_y, \tag{15}$$

where $\nabla^2 = \partial_x^2 + \partial_z^2$ in the absence of $y$-dependence.

There is one constant of motion for individual particles orbits, the canonical momentum in the $y$-direction

$$P_y = m_p V_y + \frac{eA_y}{c} = \text{constant}. \tag{16}$$

Equations (12), (15), and (16) may be combined to give the field equation for the problem

$$\left(-\nabla^2 + \frac{\omega_{pp}^2}{c^2}\right)A_y = \frac{\omega_{pp}^2}{c^2}\frac{\bar{P}_y c}{e}, \tag{17}$$

with $\omega_{pp}$ denoting the proton plasma frequency, which is a variable

$$\omega_{pp}^2 = \frac{4\pi n_p e^2}{m_p}. \tag{18}$$

The field equation has to be solved in conjunction with the two remaining components of the momentum equation for the individual proton orbits, which after the elimination of $V_y$ can be written in the following convenient notation

$$m_p\frac{d\boldsymbol{V}}{dt} = -\nabla\left\{\left[\frac{1}{m_p}\left(\frac{eA_y}{2c}\right)^2 - \frac{eA_y}{2c}P_y\right]\right\}. \tag{19}$$

Note that $A_y$ is a function of time in this equation, so energy is *not* a conserved quantity here.

The above equations model the evolution of a magnetized plasma with translation symmetry in one direction, and, in contrast to the MHD description, take into account the effect of finite proton gyroradius and frequency. The model also reproduces sound and Alfvén waves, slow modes and fast modes. Numerical simulations have been done for the geomagnetic tail (Hamilton 1976, 1980; see Hockney and Eastwood 1988, chap. 9-4, for an overview) and they demonstrate clearly the formation of a current sheet when particles are injected into an originally current-free $X$-type magnetic field configuration. It is further found that the sheet configuration is unstable for a cross-sheet field component ($B_p$) smaller than a certain threshold.

We note that there is a natural length scale in the field equation (17), $l = (c/\omega_{pp})$, that will probably determine the thickness of the current sheet. This length scale is only dependent on the density through equation (18). With the typical values of Table 1 we find $l \approx 10^8$ cm for the geotail, and $l \approx 300$ cm for the solar current sheet, in both cases close to the thickness of the current sheet, obtained from the induction equation (8). Comparison between the expressions for $\delta$ and $l$ shows this equality is not at all trivial. This fortunate coincidence further suggests that the results for the evolution

of the current sheet in the geomagnetic tail can be scaled directly to the current sheet of a two-ribbon flare.

We have formalized this by considering the dimensionless model equations. First we introduce the following parameter and units:

$$\varepsilon = \frac{B_p}{B_s}, \qquad t_0 = \frac{m_p c}{eB_s}, \qquad V_0 = \frac{E_0 c}{B_p}. \tag{20}$$

Hence the time unit is the inverse proton gyrofrequency, the velocity is normalized such that the final velocity is of the order unity, and the initial (thermal) velocity and drift velocity are very small for both the geotail and the solar corona. The parameter $\varepsilon$ expresses the dominance of the sheet magnetic field over the perpendicular field. The dimensionless equations of motion become

$$\begin{aligned} \ddot{x} &= \dot{y} f(x,z,t), \\ \ddot{y} &= \varepsilon h(x,z,t) + \varepsilon \dot{z} g(x,z,t) - \dot{x} f(x,z,t), \\ \ddot{z} &= -\varepsilon \dot{y} g(x,z,t). \end{aligned} \tag{21}$$

The functions $f$, $g$, $h$ represent, respectively, $B_z$, $B_x$, and $E_y$, and form the partial derivatives of the dimensionless potential $A(x, z, t)$. By construction they are all of order unity. The $\varepsilon$ values for the geotail and the corona are given in Table 1.

Having introduced a unit for time and velocity, the unit for length is automatically determined

$$l_0 = V_0 t_0 = \frac{m_p c^2 E_0}{B_p B_s e}. \tag{22}$$

Introducing this in the field equation (17), and using the obvious definition

$$P_{y,0} = \frac{eA_{y,0}}{c}, \tag{23}$$

one finds

$$(-\nabla^2 + \alpha n) A = \alpha n P. \tag{24}$$

Here a new parameter $\alpha$ is introduced,

$$\alpha = \frac{4\pi \bar{n}_p E_0^2 m_p c^2}{(B_p B_s)^2}. \tag{25}$$

For the geotail the value is 0.33, for the two-ribbon flare 0.43.

Thus the only two relevant parameters in this problem, $\varepsilon$ and $\alpha$, are quite similar in value for the geotail and the corona. Hence the numerical results for the evolution of the geomagnetic tail can simply be scaled to those for the corona, with the use of the physical units given above. Hamilton's (1980) simulations confirm Speiser's (1965) results for single particle trajectories. Hamilton's results further demonstrate the formation of a quasi-stationary current sheet for parameter values appropriate for the geomagnetic tail. In addition, it is demonstrated that for an $\varepsilon$-value below a certain threshold the reconnection process is nonstationary, with intermittent bursts, and the generation of multiple X- and O-type neutral lines in the sheet. The O-type configurations have strong electric fields along their axes and tend to confine and accelerate particles to extremely high energies, up to the full potential drop along the current sheet. These results are not inconsistent with the observed nature of the hard X-ray emission in two-ribbon flares, but we have not been able to apply Hamilton's instability criterion in a meaningful way to the impulsive phase of flares. This subject will be studied in future detailed numerical simulations for flares with Hamilton's code.

## V. CONCLUSIONS

We have argued that there is a great similarity between the physical situation of the geomagnetic tail and the current sheet in the wake of an erupting filament. We have demonstrated that the dimensionless parameters characterizing these plasmas are of similar value, and that the existence of super Dreicer fields in the solar corona is plausible. In the final analysis the similarity between the solar current sheet and the geotail goes so far that the dimensionless evolution equations for both systems, under the assumption of invariance along the sheet axis, and dominance of proton currents, have similar constants. Consequently the results for the numerical simulations of the geotail (Hamilton 1980) can be scaled to the corona.

Further we have reviewed the observational material pertinent to both neutral beams with hekta KeV protons, and standard deka KeV electron beams. We find that in addition to Simnett's (1986) arguments for neutral beams, two independent sets of line polarization measurements (Hénoux *et al.* 1983, 1990) seem to rule out standard electron beams in favor of neutral beams. However, the observations are still too few, and their interpretation is not yet sufficiently established.

Future measurements of line polarization—either ground-based H$\alpha$ or UV space observations—are clearly desirable, as well as high spectral and temporal resolution measurements of redshifted Ly$\alpha$, advocated by Canfield and Chang (1985). On the theoretical side, the application of codes developed for the geomagnetic tail to solar type sheets is called for.

A. Y. acknowledges stimulating discussions with Robert Rosner in the early stages of this work. P. M. acknowledges helpful and informative discussions with Jean-Claude Hénoux. We thank the referee for suggesting Figure 1 and other important improvements in this paper.

Studies of coronal plasma processes at the Harvard-Smithsonian Center for Astrophysics are supported by NASA grant NAGW-112.

## REFERENCES

Akasofu, S.-I., Hones Jr., E. W., Bame, S. J., Asbridge, J. R., and Lui, A. T. Y. 1973, *J. Geophys. Res*, **78**, 7257.
Antonucci, E., *et al.* 1982, *Solar Phys.* **78**, 107.
Antonucci, E. Gabriel, A. H., and Dennis, B. R. 1984, *Ap. J.*, **287**, 917.
Anzer, U., and Pneuman, G. W. 1982, *Solar Phys.*, **79**, 129.
Canfield, R. C. 1988, private communication.
Canfield, R. C., Chang, C-R 1985, *Ap. J.*, **295**, 275.
Canfield, R. C., and VanHoosier, M. E. 1980, *Solar Phys.*, **67**, 339.
Carmichael, H. 1964, *AAS-NASA Symposium on the Physics of Solar Flares*, NASA SP-50, ed. W. N. Hess (Washington, DC: NASA), p. 451.
Chupp, E. L., *et al.* 1982, *Ap. J.* (*Letters*), **263**, L95.

Cliver, E. W., Dennis, B. R., Kiplinger, A. L., Kane, S. R., Neidig, D. F., Sheely, N. R., and Koomen, M. J. 1986, *Ap. J.*, **305**, 920.
Dennis, B. R. 1985, *Solar Phys.*, **100**, 465.
_____. 1988, *Solar Phys.*, **118**, 49.
Duijveman, A., Hoyng, P., and Machado, M. E. 1982, *Solar Phys.*, **81**, 137.
Eastwood, J. W. 1972, *Planetary Space Sci.*, **20**, 1555.
_____. 1974, *Planetary Space Sci.*, **22**, 1641.
Elliot, H. 1964, *Planetary Space Sci.*, **12**, 657.
Fisher, G. H. 1987, *Ap. J.*, **317**, 502.
Fisher, G. H., Canfield, R. C., and McClymont, A. M. 1985, *Ap. J.*, **289**, 425.
Forbes, T. G., and Priest, E. R. 1984, in *Solar Terrestrial Physics: Present and Future*, NASA-SP 1120, ed. D. M. Butler and K. Papadopoulos (Washington, DC: NASA), p. 1.
Forrest, D. J., *et al.* 1981, in *Proc. 17th Internat. Cosmic Ray Conf.*, (Paris) **10**, 5.
Foukal, P., Hoyt, C., and Gilliam, L. 1986, *Ap. J.*, **303**, 861.
Foukal, P., Miller, P., and Gilliam, L. 1983, *Solar Phys.*, **83**, 83.
Foukal, P., Little, R., and Gilliam, L. 1987, *Solar Phys.*, **114**, 65.
Hamilton, J. M. 1976, *Reading University Computer Science Report*, No. RCS 9.
_____. 1980, Ph.D. thesis, University of Reading.
Hénoux, J. C. 1990, *Ap. J. Suppl.*, this issue.
Hénoux, J. C., *et al.* 1983, *Ap. J.*, **265**, 1066.
Hénoux, J. C., and Chambe, G. 1990, *J. Quant. Spectros. Rad. Transf.*, in press.
Hénoux, J. C., Chambe, G., Feautrier, N. Sahal, S., and Rovira, M. 1990, *Nature*, submitted.
Heristchi, D., and Trottet, G. 1971, *Phys. Rev. Letters*, **26**(4), 197.
Heristchi, D., Trottet, G., and Perez-Peraza, J. 1976, *Solar Phys.*, **49** 151.
Hockney, R. W., and Eastwood, J. W. 1988, *Computer Simulations Using Particles* (Philadelphia: Hilger).
Hoyng, P., Brown, J. C., and Van Beek, H. F. 1976, *Solar Phys.*, **48**, 197.
Hoyng, P., *et al.* 1981, *Ap. J.* (*Letters*), **246**, L155.
Kaastra, J. S. 1985, Ph.D. thesis, University of Utrecht.
Kane, S. R., Anderson, K. A., Evans, W., Klebesadel, R., and Laros, J. 1980, *Ap. J.* (*Letters*), **239**, L85.
Kopp, R. A., and Pneuman, G. W. 1976, *Solar Phys.*, **50**, 85.
Kopp, R. A., and Poletto, G. 1986, *Coronal and Prominence Plasmas*, NASA-CP 2442, ed. A. Poland (Washington, DC: NASA) p. 469.
Lin, R. P., and Schwartz, R. A. 1987, *Ap. J.*, **312**, 462.
Lundin, R., Hultqvist, B., Pissarenko, N., and Zackarov, A. 1981, preprint.
Lyons, L. R., and Speiser, T. W. 1985, *J. Geophys. Res.*, **90**, 8543.
Lyons, L. R., and Williams, D. J. 1984, *Quantitative Aspects of Magnetospheric Physics*, (Dordrecht: Reidel).
MacKinnon, A. L., Brown, J. C., and Hayward, J. 1985, *Solar Phys.*, **99**, 189.
Martens, P. C. H. 1988*a*, *Ap. J.* (*Letters*), **330**, L131.
_____. 1988*b*, in: *Solar and Stellar Coronal Structure and Dynamics*, ed. R. C. Altrock (Sunspot, NM: National Solar Observatory), p. 501.
Martens, P. C. H., and Young, A. 1989, in *Nonlinear Effects in Vlasov Plasmas*, ed. F. Doveil (Orsay, Editions de Physique), p. 381.
Martens, P. C. H., and Kuin, N. P. M. 1989, *Solar Phys.*, **122**, 263.
Mikic, Z., Barnes, D. C., and Schnack, D. D. 1988, *Ap. J.*, **328**, 830.
Ness, N. F. 1965, *J. Geophys. Res.*, **70**, 2989.
Orral, F. Q., and Zirker, J. B. 1976, *Ap. J.*, **208**, 618.
Pneuman, G. W. 1980, in *IAU Symposium*, **91**, *Solar and Interplanetary Dynamics*, eds. M. Dryer and E. Tanberg-Hanssen (Dordrecht: Reidel), p. 317.
Poletto, G., Vaiana, G. S., Zombeck, M. V., Krieger, A. S., and Timothy, A. F. 1975, *Solar Phys.*, **44**, 83.
Ramathy, R., and Murphy, R. J. 1984, in *High-Energy Transients in Astrophysics*, ed. S. Woosley (New York: A. I. P.), p. 628.
Rosenbauer, H. A., Grunwaldt, M. D., Montgomery, G., Paschmann, G., and Sckopke 1975, *J. Geophys. Res.*, **80**, 2723.
Rosner, R., Tucker, W. H., and Vaiana, G. S. 1978, *Ap. J.*, **220**, 643.
Schatzman, E. 1967, *Solar Phys.*, **1**, 411.
Simnett, G. M. 1986, *Solar Phys.*, **106**, 165.
Simnett, G. W., and Strong, K. T. 1984, *Ap. J.*, **284**, 839.
Sivukhin, D. V. 1965, in *Reviews of Plasma Physics*, Vol. **1**, ed. M. A. Leontovich (New York: Consultants Bureau), p. 1.
Speiser, T. W. 1965, *J. Geophys. Res.*, **70**, 4219.
_____. 1967, *J. Geophys. Res.*, **72**, 3919.
_____. 1968, *J. Geophys. Res.*, **73**, 1112.
Speiser, T. W. 1984, *Adv. Space Res.*, **4**, 439.
_____. 1987, *Phys. Scripta*, **T18**, 119.
Speiser, T. W., and Ness, N. F. 1967, *J. Geophys. Res.*, **72**, 131.
Stenzel, R. L., Gekelman, W., and Urrutia, J. M. 1985, in *Magnetic Reconnection and Turbulence*, ed. M. A. Dubois, D. Gresillon, and M. N. Bussac (Orsay: Editions de Physique), p. 63.
Stenzel, R. L., Gekelman, W., and Wild, N. 1983, *J. Geophys. Res.*, **88**, 4793.
Takakura, T., Tanaka, K., Nitta, N., Kai, K., and Ohki, K. 1986, *Solar Phys.*, **107**, 109.
Tramiel, L. J., Chanan, G. A., and Novick, R. 1984, *Ap. J.*, **280**, 448.
Trubnikov, B. A. 1965, in *Reviews of Plasma Physics*, Vol. **1**, ed. M. A. Leontovich (New York: Consultants Bureau), p. 105.
Van Tend, W., and Kuperus, M. 1978, *Solar Phys.*, **59**, 115.
Vilmer, N. 1987, *Solar Phys.*, **111**, 207.

P. C. H. MARTENS and A. YOUNG: Harvard-Smithsonian Center for Astrophysics, 60 Garden Street, Cambridge, MA 02138